EXPERIMENTAL INVESTIGATION OF HYDROGEN RELEASE AND IGNITION FROM FUEL CELL POWERED FORKLIFTS IN ENCLOSED SPACES

Ekoto, I.W.[1], Merilo, E.G.[2], Houf, W.G.[1], Evans, G.H.[1], and Groethe, M.A.[2]
[1] Sandia National Laboratories, Livermore, CA 94551-0969, USA, iekoto@sandia.gov
[2] SRI International, Menlo Park, CA 94025, USA, erik.merilo@sri.com

ABSTRACT

Due to rapid growth in the use of hydrogen powered fuel cell forklifts within warehouse enclosures, Sandia National Laboratories has worked to develop scientific methods that support the creation of new hydrogen safety codes and standards for indoor refueling operations. Based on industry stakeholder input, conducted experiments were devised to assess the utility of modeling approaches used to analyze potential consequences from ignited hydrogen leaks in facilities certified according to existing code language. Release dispersion and combustion characteristics were measured within a scaled test facility located at SRI International's Corral Hollow Test Site. Moreover, the impact of mitigation measures such as active/passive ventilation and pressure relief panels was investigated. Since it is impractical to experimentally evaluate all possible facility configurations and accident scenarios, careful characterization of the experimental boundary conditions has been performed so that collected datasets can be used to validate computational modeling approaches.

1 INTRODUCTION

Initial commercialization of hydrogen (H_2) gas as an alternative transportation fuel is occurring within the material handling sector as H_2 fuel cells replace lead-acid batteries for indoor use industrial forklifts. However, compressed H_2 indoor refueling within enclosed spaces introduces new operational considerations that must be addressed to enable widespread deployment. Sandia National Laboratory's Hydrogen Safety, Codes and Standards research group has collaborated with original equipment manufacturers (OEMs) to develop and evaluate the scientific underpinnings for risk-informed, safety standards. According to LaChance et al. [1], the principal hazard associated with the use of compressed H_2 is the uncontrolled release within a confined space followed by ignition of the flammable H_2/air mixture. To address these concerns, the 2011 edition of NFPA 2 [2] limits indoor H_2 dispensing rates within unventilated warehouses to 0.8 kg per 1,000 m^3 of room volume, provided a minimum 7.62 m ceiling height is met. Room volume requirements are exempted, however, if threshold mechanical ventilation rates are maintained (83.3 liters/min per cubic meter of room volume). A combined numerical and experimental approach has been used to develop validated modeling methods that can be used by the standards development community to provide technical assessments of these guidelines. The current paper summarizes the experimental results, while simulation findings are described by Houf et al. [3].

Previous studies have examined H_2 releases within confined spaces, both with and without ignition of the flammable mixtures [4-7], and have assessed the impact of active/passive ventilation systems on H_2 dispersion characteristics and ignition behavior [8-13]. Based on the study results, active exhaust requirements have been incorporated into existing fire codes (e.g., NFPA 2 [2], NFPA 52 [14], and the International Fire Code [15]) for the safe utilization of H_2 within enclosed spaces. Most of these studies, however, examined either lean homogeneous mixtures or steady releases at low flow rates, and did not consider more substantial transient blowdowns from compressed storage applications.

For the present validation experiments, realistic H_2 dispersion behavior and combustion phenomena that result from a medium sized leak with subsequent ignition were examined within a scaled enclosure. The release scenario was defined based on industry forklift specifications, current NFPA 2 indoor refueling guidelines, and a failure mode and effects analysis (FMEA) that was developed with OEM consultation. Such a complex scenario was necessary as a validation benchmark to ensure developed modeling approaches were capable of capturing all observed phenomena. For the devised scenario, 0.8 kg of compressed H_2 stored at 35 MPa (typical of full Class 3 fuel cell forklift tanks) was released into a 1,000 m^3 warehouse enclosure and ignited after a short ignition delay (~5 s). The compressed hydrogen was assumed to be released through a 6.35 mm opening that could either represent the medium sized leak from the FMEA or a release via the storage tank's thermally activated pressure relief device (TPRD). Hydrogen then exited into the warehouse through a grill on the forklift side. The spark source was located either just above the forklift where mixtures could be autoignited (e.g., from hot surfaces, electrostatic discharge, or shock heating [16]) or near the ceiling where non-explosion proof electrical components could act as an ignition source. Hydrogen release concentrations were obtained from oxygen (O_2) depletion measurements using strategically distributed fast-response O_2 sensors. Infrared (IR) visualization was performed on the facility open end so that flame front development could be observed. Finally, the facility open end was replaced by a rigid steel wall, and overpressure and flame front time-of-arrival (TOA) measurements were recorded from distributed pressure transducers and high-speed thermocouples. The effect of ventilation was investigated through variations in both passive effective leakage area and active mechanical ventilation rate. Pressure relief panels with different yield values were also examined.

2 EXPERIMENTAL SETUP

2.1 Scaled Test Facility

All experiments were performed in a subscale test facility located at the SRI Corral Hollow Experiment Site in Livermore California, which measured 3.64 m wide, 4.59 m long, 2.72 m high, and had a total internal volume, V, of 45.4 m^3. A photograph of the test facility is provided in Fig. 1, while a schematic of the warehouse geometry is given in Fig. 2. The facility was well suited for the desired measurements because of its blast hardened walls and geometric features that favorably scaled to the full scale 1,000 m^3 internal volume and 7.62 m ceiling height if the Froude scaling relations developed by Hall and Walker [17] were applied. The scaling approach has been successfully applied in previous dispersion and deflagration tests within a partially enclosed tunnel [5]. For this scaling methodology, the scale factor, *SF*, is equivalent to the cube-root of the ratio of subscale (*SS*) and full scale (*FS*) internal volumes, and is equal to 0.36 for the examined configuration. Additional quantities of interest include the release time, t, release rate, Q, and total H_2 mass, m. Normalized Froude scaling for each parameter as a function of *SF* are as follows:

$$\frac{V_{SS}}{V_{FS}} = (SF)^3;\ \frac{t_{SS}}{t_{FS}} = (SF)^{\frac{1}{2}};\ \frac{Q_{SS}}{Q_{FS}} = (SF)^{2.5};\ \frac{m_{SS}}{m_{FS}} = (SF)^3 \quad (1)$$

Figure 1. Photograph of the SRI subscale warehouse test facility.

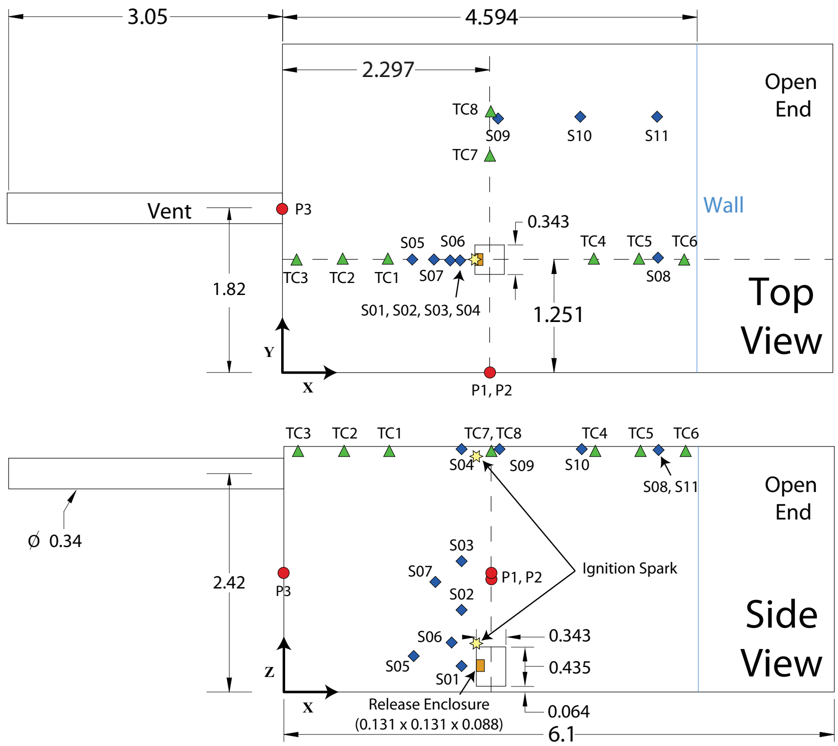

◆ Concentration Sensors

Sensor	X [m]	Y [m]	Z [m]
S01	1.97	1.25	0.28
S02	1.97	1.25	0.90
S03	1.97	1.24	1.44
S04	1.97	1.25	2.68
S05	1.44	1.25	0.39
S06	1.86	1.24	0.54
S07	1.68	1.25	1.21
S08	4.16	1.27	2.67
S09	2.39	2.81	2.68
S10	3.30	2.83	2.68
S11	4.15	2.83	2.67

● Pressure Sensors

Sensor	X [m]	Y [m]	Z [m]
P1†	2.30	0.00	1.30
P2	2.30	0.00	1.24
P3	0.00	1.81	1.31

†P1 was not used for Test 7

▲ Thermocouples

Sensor	X [m]	Y [m]	Z [m]
TC1	1.17	1.26	2.66
TC2	0.67	1.26	2.66
TC3	0.16	1.25	2.66
TC4	3.45	1.26	2.66
TC5	3.95	1.26	2.66
TC6	4.45	1.25	2.66
TC7	2.30	2.40	2.66
TC8	2.31	2.89	2.66

☆ Ignition Spark

Location	X [m]	Y [m]	Z [m]
Forklift	2.13	1.42	0.53
Ceiling	2.13	1.42	2.62

Figure 2. Scaled warehouse schematic with the forklift model placement and sensor/spark locations.

For the release scenario described in the introduction, the full scale tank blowdown was modeled as an isentropic expansion through a 6.35 mm choked orifice using the NETFLOW compressible network flow analysis code [18]. Subscale release characteristics were derived using the Froude scaling relations (Eq. 1), while tank specifications, orifice sizing, and initial conditions were selected to provide the best match with the calculations. Since peak storage pressures for industrially packed compressed hydrogen cylinders used in the present study were limited to around 13.7 MPa, the orifice size was accordingly increased to match the desired flow rate. Full and subscale calculated release rates are compared to measured subscale release rates in Fig. 3, while full and subscale tank characteristics are summarized in Table 1.

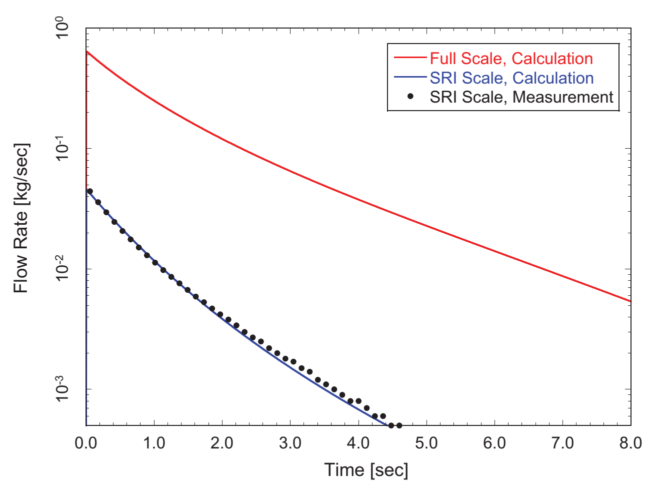

Figure 3. Calculated full (red) and subscale (blue) release rates along with a comparison of measured SRI subscale release rates (filled circles).

Table 1. Tank specifications and initial conditions.

	Full scale	Subscale
Tank Volume [liters]	33.9	3.63
Tank Pressure [MPa]	35	13.45
Tank Temperature [K]	294	297
Hydrogen Mass [kg]	0.80	0.0363
Release Diameter [mm]	6.35	3.56[†]

[†]0.75 discharge coefficient

2.2 Forklift Model

The forklift model, constructed from 3.2 mm thick steel and scaled to match OEM specifications, measured 34.3 cm long, 34.3 cm wide, 43.5 cm high, and was elevated 6.4 cm off the facility floor. Large interior voids were filled with sand, while small gaps were sealed with spray foam and tape to prevent H_2 from filling the internal volume. A detailed diagram and photograph of the forklift model and H_2 delivery system are shown in Fig. 4. Pressurized H_2 was stored in a modified nitrous oxide bottle that was connected to the release valve with high-pressure stainless steel lines. Tank pressure was monitored with an Omega MMSG2.5KV10P4C1T3A5 piezoresistive pressure transducer, while tank temperature was measured using a Type-K thermocouple. Commercial hydrogen "six-packs" were used to fill the modified H_2 cylinder to the desired 13.5 MPa pressure prior to each test. A Tescom VG-C6CBVG9H9 air-operated valve with a ~75 ms actuation time was used to initiate the release through a 3.56 mm brass orifice nozzle. To replicate the nearly uniform release characteristics through the forklift side grate described for the full scale scenario in the introduction, hydrogen was released toward the back of a 13.1 cm wide, 13.1 cm high, and 8.8 cm deep enclosure located on the model side orientated in the -X direction (see Fig. 2). To further straighten the flow, the enclosure was packed with 3.175 mm diameter steel beads that reduced the internal volume to 590 cm^3. A porous frit was used to prevent steel beads from clogging the orifice, and the beads were kept in the release enclosure by a perforated steel plate with 1.91 mm holes and a 51% open area.

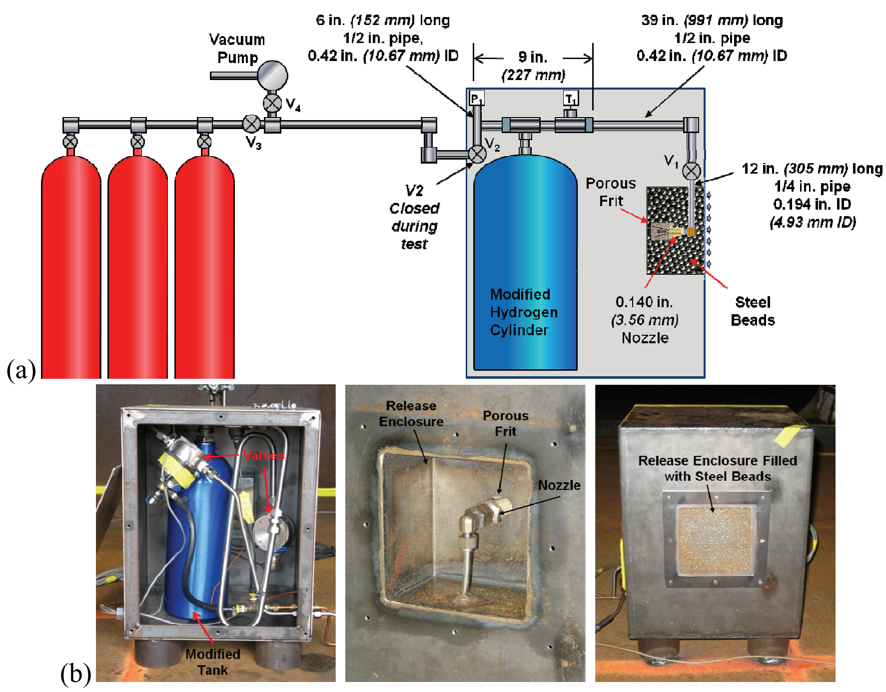

Figure 4. (a) Schematic of the H_2 delivery system and (b) an image of forklift model with the modified H_2 storage tank, fast-opening valves, release nozzle and porous frit.

2.3 Test Procedures and Matrix

The test series was broken down into 3 phases. The first phase was used to quantify H_2 release dispersion characteristics using concentration sensors distributed along the expected release plume, determined from FUEGO computational simulation results [19], and across the ceiling (see Fig. 2). The identified release scenario was initially performed without mechanical ventilation (Test 1) and then repeated (Test 2) so that test-to-test mixture variability could be examined. The release scenario was then repeated with active warehouse ventilation at the rate specified by NFPA 2 and described in the introduction, so that the influence of mechanical ventilation on release dispersion could be assessed (Test 3). A FLACS deflagration [20] model was used simulate cloud ignition at different locations. For the second test phase, concentration sensors were removed and qualitative visualization of flame front development was performed through IR imaging. From the FUEGO/FLACS simulation predictions, the ignition locations with the highest overpressures were directly above the grill side forklift edge (Fig. 2) either 3 cm above the top of the forklift model (Test 4 and 5) or 10 cm below the ceiling (Test 6); spark points were accordingly placed in these locations. For the final test phase (Tests 7 through 13), overpressure and flame speed data were recorded with the facility open end replaced by a rigid steel wall that was sturdy enough to withstand the expected overpressures generated from the expansion of hot product gasses. A 2.4 m by 1.2 m opening provided access to the facility internal volume and allowed up to three 1.27 cm thick plywood pressure relief panels to be installed. Ignition location/delay, ventilation area, exhaust rate, and the robustness of the pressure relief panel were all varied. A summary of all conditions is provided in Table 2.

Table 2. Test matrix and description.

Test	Wall	Pressure Relief Panel Support	Ventilation Area [cm^2]	Ventilation Rate [m^3/min]	Ignition Location	Ignition Delay [s]
1	HDPE	N/A	86.5±5.0%	N/A	N/A	N/A
2	HDPE	N/A	86.5±5.0%	N/A	N/A	N/A
3	HDPE	N/A	995.5±3.3%	6.5	N/A	N/A
4	HDPE	N/A	86.5±5.0%	N/A	Near Forklift	3.0
5	None	N/A	N/A	N/A	Near Forklift	3.0
6	None	N/A	N/A	N/A	Ceiling	3.5
7	Steel	Wood Screws	109.7±1.0%	N/A	Near Forklift	3.0
8	Steel	Bolted Wood Frame	39.4±1.1%	N/A	Near Forklift	3.0
9	Steel	Bolted Wood Frame	39.4±1.1%	N/A	Ceiling	3.5
10	Steel	Bolted Wood Frame	971.6±4.2%	6.3	Near Forklift	3.0
11	Steel	Bolted Wood Frame	971.6±4.2%	Natural	Near Forklift	3.0
12	Steel	Reinforced Wood Frame	36.8±1.4%	N/A	Near Forklift	3.0
13	Steel	Reinforced Wood Frame	36.8±1.4%	N/A	Ceiling	3.5

2.4 Open Wall Configurations

Different facility open end wall arrangements were used to facilitate data acquisition and allowed an examination of various ventilation and pressure relief panel configurations. The facility open end was covered with an 8 μm thick high-density polyethylene (HDPE) sheet (Fig. 5a) for all dispersion tests. For all overpressure scenarios except Test 7, an external wooden frame was used to secure the plywood pressure relief panel to the steel wall (Fig. 5b); for Tests 12 and 13 the panel was further reinforced with Unistrut mounted across the surface (Fig. 5c). A 120 cm by 6.35 cm rectangular vent was located below the relief panel (Fig. 5d) for the overpressure tests with ventilation, and functioned as the air inlet for the mechanical exhaust. A 34 cm diameter circular vent was located at the upper end of the rear exhaust duct. Two variable-speed muffin fans that were mounted at the duct exit were used to generate the desired ventilation rates. Duct velocities were measured 2.75 m downstream from the duct inlet at 7 separate radial locations, and were normalized in proportion to their represented duct area so that the average bulk flow ventilation rate could be calculated. For conditions without active exhaust, the duct inlet was sealed by a steel plate with tape along the seams.

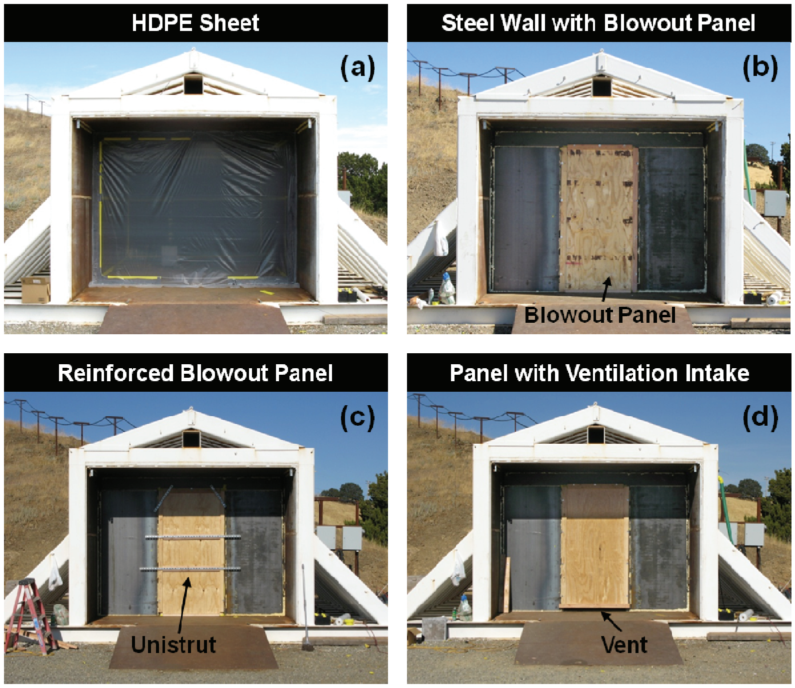

Figure 5. Warehouse open end wall configurations.

2.5 Instrumentation and Test Procedures

Hydrogen concentrations were derived from O_2 depletion measurements acquired from 11 fuel cell based Teledyne Electronic Technologies UFO-130 sensors that were distributed along the expected plume release path and across the facility ceiling; location details are given in Fig. 2. These sensors were selected because they are insensitive to flow variations and have fast response times (~100 msec) relative to commercially available H_2 sensors. The sensors were calibrated prior to each test and H_2 mole fractions were calculated using:

$$\chi_{H_2} = 1 - \chi_{O_2} - \left(\chi_{O_2}/\chi_{O_2,air}\right)\left(\chi_{H_2O,air} + \chi_{other,air}\right) \tag{2}$$

where χ_{O_2} is the detected O_2 mole fraction, and the variables $\chi_{O_2,air}$, $\chi_{H_2O,air}$, and $\chi_{other,air}$ were the respective O_2, water vapor, and other constituent mole fractions for air. Weather conditions, including relative humidity, were continuously monitored and logged by a Davis Vantage Pro weather station.

Fast-response coaxial thermocouples (Medtherm Type E Model TCS-061-E-1.00-NI-GGSZ-A1-0), located 6.0 cm below the warehouse ceiling, were used to measure the flame front TOA. The thermocouple junctions were directed away from the spark location so that measurements were not influenced by thermal radiation. For overpressure measurements, Honeywell TJE, Tescom 100-30-2127, and Tescom 100-5-2127 piezoresistive transducers were used.

Instrumentation output voltages were recorded by Nicolet Odyssey data recorders at a 200-kHz rate, and were backed up by 20-kHz logs from Nicolet Odyssey and Nicolet 440-type recorders. A 0.2-kHz averaging filter was applied to tank pressure/temperature and warehouse concentration measurements and a 5-kHz averaging filter was applied to pressure data from sensors P2 and P3. Pressure data from sensor P1 were low-pass filtered with a 1.0-kHz cutoff frequency, and a band-reject filter was applied from 40 to 80-Hz and 100 to 300-Hz. No filtering was applied to the thermocouple data.

Flame front IR videos were recorded using a Sony HDR-HC digital camera with "Night Shot" through an X-Nite 1000B-2mm filter with a 1.0-µm cutoff at 50% and a 1.3-µm pass-band of greater than 90%. Videos during the overpressure tests were recorded by a Panasonic PV-GS31 standard video camera. Both cameras were placed in a protective shelter and pointed towards the test facility open end during testing.

Before each test, the modified storage tank and supply lines were evacuated using a rotary vane vacuum pump. The pump was then isolated and the system was filled with compressed H_2 until the system pressure and temperature stabilized. The release was initiated by opening the release valve between the modified H_2 tank and the orifice nozzle. For ignited releases, the ignition system consisted of a firing unit, delay generator, 40 J capacitive discharge unit (CDU), firing cable, and bridge wire. The delay generator sent two voltage pulses: the first to initiate the valve opening and the second to discharge the CDU after the desired ignition delay (the time between the release and the spark) had elapsed. Ignition delays were timed to occur when flammable mixtures were present at the spark location. Data acquisition for tank pressure/temperature and warehouse concentration measurements were referenced to the valve opening, while flame front TOA and overpressure measurements along with the standard and IR video were referenced to the spark time.

2.6 Facility Air Leakage Test

Scoping numerical simulations indicated that developed overpressures were sensitive to the amount of open area ventilation. Thus, a Model 3 Minneapolis Blower Door manufactured by The Energy Conservatory was used to measure the facility leakage area for each test configuration through programmable depressurization tests. A fixture was constructed so that the blower door could be mounted in the steel wall relief panel opening. A DG-700 pressure and flow gauge was used with TECTITE 3.2 software to perform the tests in "Cruise Control" mode. Leakage area results were calculated using the CGSB 149.10-M86 test standard, which consists of 8 measurements at different building pressures ranging from 50 to 15 Pa. One hundred building pressure and air flow rate samples were recorded and averaged at each of the 8 building pressures. The leakage area was taken as the shape of a sharp-edged orifice with a 10 Pa source pressure. For well-sealed conditions, the most significant leaks were detected along the blower door frame, which indicates actual facility leakage areas were likely lower. Note also that when a H_2-air deflagration occurs inside the facility, additional leakage due to facility deformation from elevated overpressures could occur. The measured exhaust tube leakage area with the muffin fans mounted in place was 197 cm^2, while the measured lower vent leakage area was 712 cm^2, which compares favorably with the actual 761 cm^2 lower vent area.

(a) 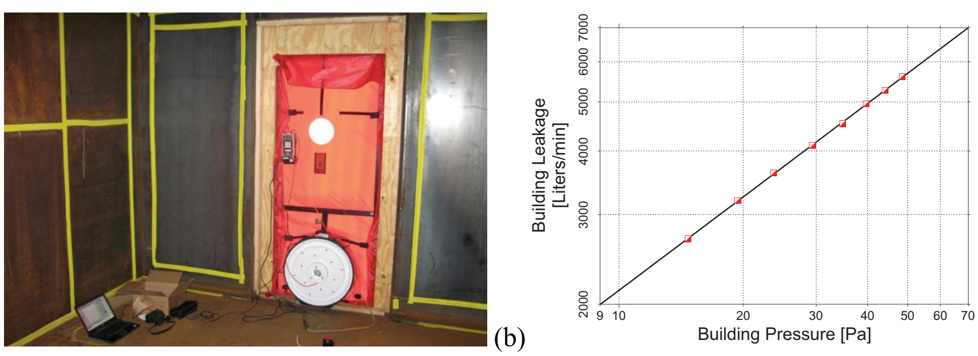 (b)

Figure 6. (a) Air leakage test setup inside the facility and (b) typical leak test results (Test 7).

3 RESULTS AND DISCUSSION

3.1 Hydrogen Dispersion

Transient H_2 concentration measurements for select sensors from each dispersion test are displayed in Fig. 7, while peak concentrations at all sensor locations are provided in Table 3. Near the release point

(Fig. 7a) a concentration spike was observed shortly after the start of the release (~100 ms), and is believed to be artificially generated from shock induced sensor movement from the valve opening. For the baseline release (Test 1) the first meaningful concentrations were detected at sensor S01, located 15 cm in front of the release enclosure, 0.15 s after the valve opened. These mixtures quickly approached H_2 mole fractions of 1.0 by 0.45 s into the release. As the release rate, and hence jet momentum, decreased, the jet steadily bent upwards and by 1.3 s into the release, H_2 concentrations in this region sharply declined. Around this same time sensor S06, located 11 cm in front of and 26 cm above sensor S01, registered flammable H_2/air mixtures; flammable mixtures were also detected at sensor S07, located 29 cm in front of and 97 cm above sensor S01, ~0.2 s later. By ~2 s into the release, negligible H_2 concentrations were measured at S01, while peak mole fractions of around 0.92 and 0.44 were measured at S06 and S07 respectively. After about 4 s, no measureable H_2 concentrations were detected near the release point. Similar results were observed for the retest (Test 2) and actively ventilated (Test 3) conditions, which indicated the moderate exhaust rates had minimal impact on initial release distributions.

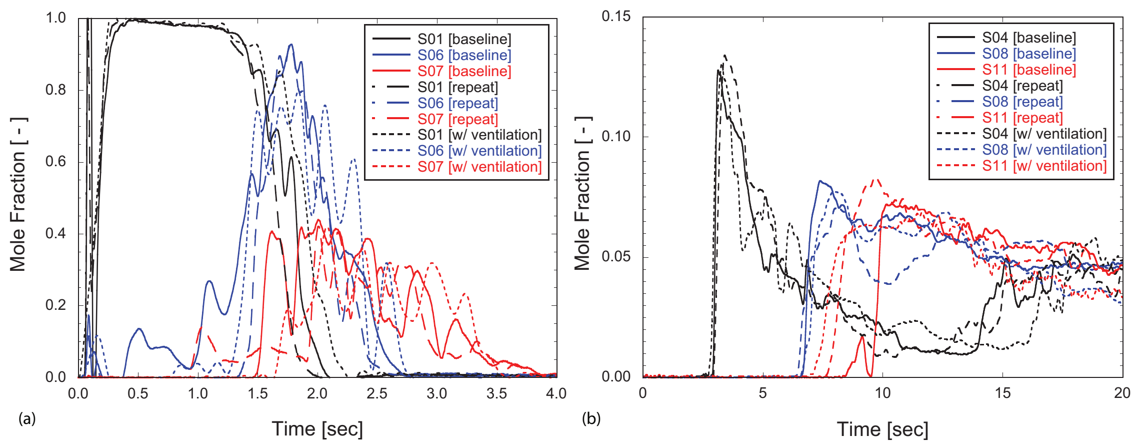

Figure 7. Hydrogen mole fractions from select sensors (a) near the release location and (b) along the ceiling, either with or without mechanical ventilation.

Time dependent H_2 mole fractions at select sensors along the ceiling are displayed in Fig. 7b for each dispersion test. Sensor S04 was mounted 2.4 m directly above sensor S01 (4 cm below the ceiling), and was the first ceiling sensor to detect H_2 concentrations at about 3 s into the release. Hydrogen mole fractions almost immediately peaked at 0.13, before steadily decreasing. Sensors S08 and S11, were located next to the test facility open end and peak H_2 mole fractions of around 0.08 occurred between 7 and 10 seconds after the release was initiated. After 30 seconds all ceiling sensors measured H_2 mole fractions near 0.04. Test-to-test variations between all tests continued to be minimal, which indicated the releases were highly repeatable at all locations throughout the warehouse and the impact of ventilation was minimal for several seconds into the release.

Table 3. Peak H_2 mole fractions at each sensor location for dispersion Tests 1 through 3.

Test	S01	S02	S03	S04	S05	S06	S07	S08	S09	S10	S11
1	1.000	0.336	0.187	0.128	0.917	0.923	0.441	0.082	0.090	0.067	0.072
2	1.000	0.510	0.164	0.134	0.860	0.916	0.400	0.071	0.081	0.071	0.083
3	1.000	0.576	0.225	0.131	0.895	0.797	0.420	0.077	0.076	0.059	0.069

3.2 Flame Front Imaging

Initial IR imaging was performed through the HDPE sheet (Test 4) so that pre-ignition mixtures would not be disturbed by the wall absence. However, it was determined after examination of the video and concentration measurements that mixtures near the facility open end were too lean to ignite, and the sheet was removed for subsequent tests to improve image clarity. Only images from the tests without the HDPE sheet are shown. Figure 8a displays select IR images from Test 5, where ignition was initiated 3 cm above the forklift model after a 3.0 s ignition delay. A highly luminous flame was observed traveling upward along the H_2-rich release plume. After a ~0.4 s ignition dwell period, a secondary ignition of accumulated lean mixture occurred along the upper left facility corner. Most heat release was complete by roughly 1 s after ignition, except for residual release enclosure H_2 that continued to burn. Note that IR images from the test with the HDPE sheet were qualitatively similar.

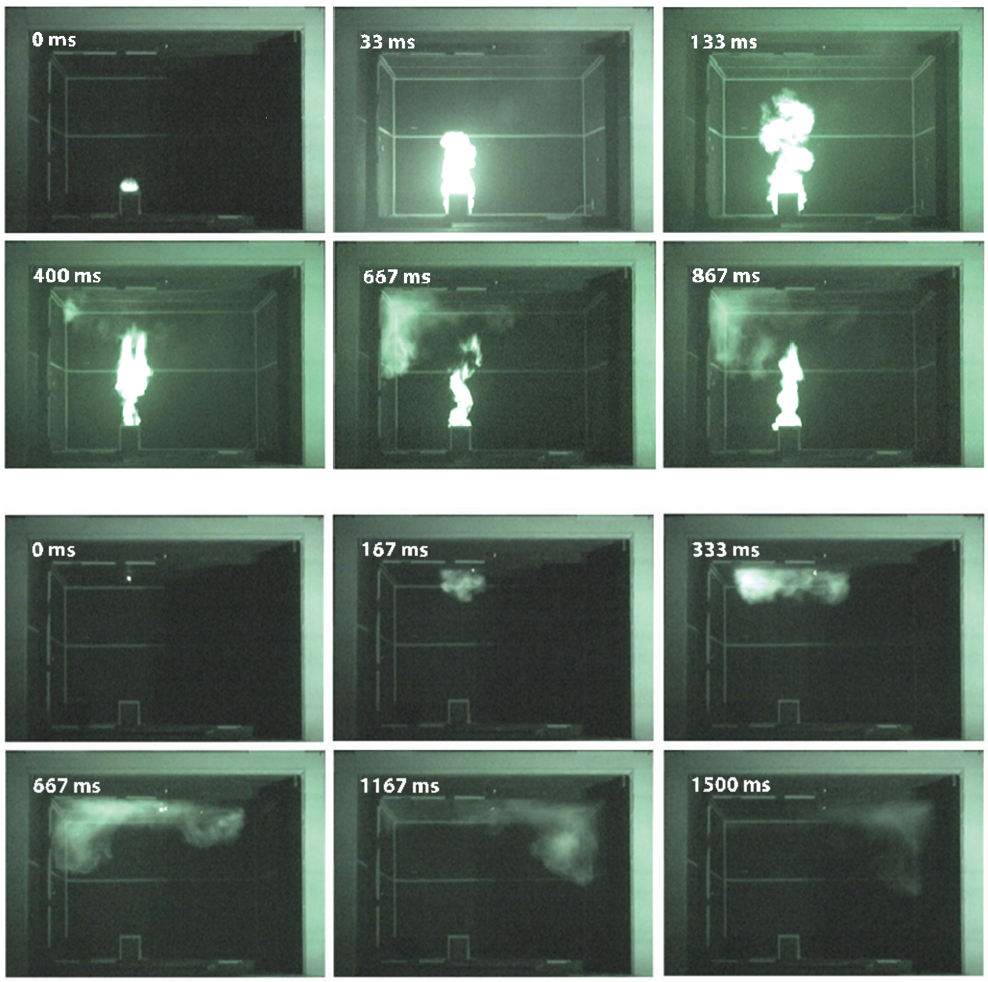

(a)

(b)

Figure 8. (a) Forklift (Test 5) and (b) ceiling (Test 6) ignition scenario infrared image sequences.

Figure 8b shows select video frames from the ceiling ignition condition (Test 6) with a 3.50 s ignition delay. Since ignited mixtures were lean, kernel development and flame front propagation along the ceiling was relatively slow; no flame propagation towards the forklift model was observed along the release plume. When the flame approached the walls, it was directed downward with the maximum extent reaching halfway down the facility. The asymmetric flame propagation likely resulted from richer mixture accumulating on the warehouse left side due to the offset forklift model orientation.

3.3 Overpressure Measurements

Seven confined deflagration tests were performed with the warehouse open end sealed by a steel wall and pressure relief panel assembly, as described in the experimental setup section. A comparison of transient warehouse overpressures measured from sensor P1 for Test 7 and P2 for all other tests is given in Fig. 9. Pressure variations from all sensors were within ~0.1 kPa. For well-sealed warehouse conditions (Tests 7, 8, 9, 12 and 13), the initial 1 kPa pressure rise that occurred before ignition was attributed to the expansion of the released H_2. Flame front TOA was measured in 3 directions by fast-response thermocouples located 6 cm below the ceiling, and were used to compute the horizontal flame speed component. Results are summarized in Table 4 for all conditions.

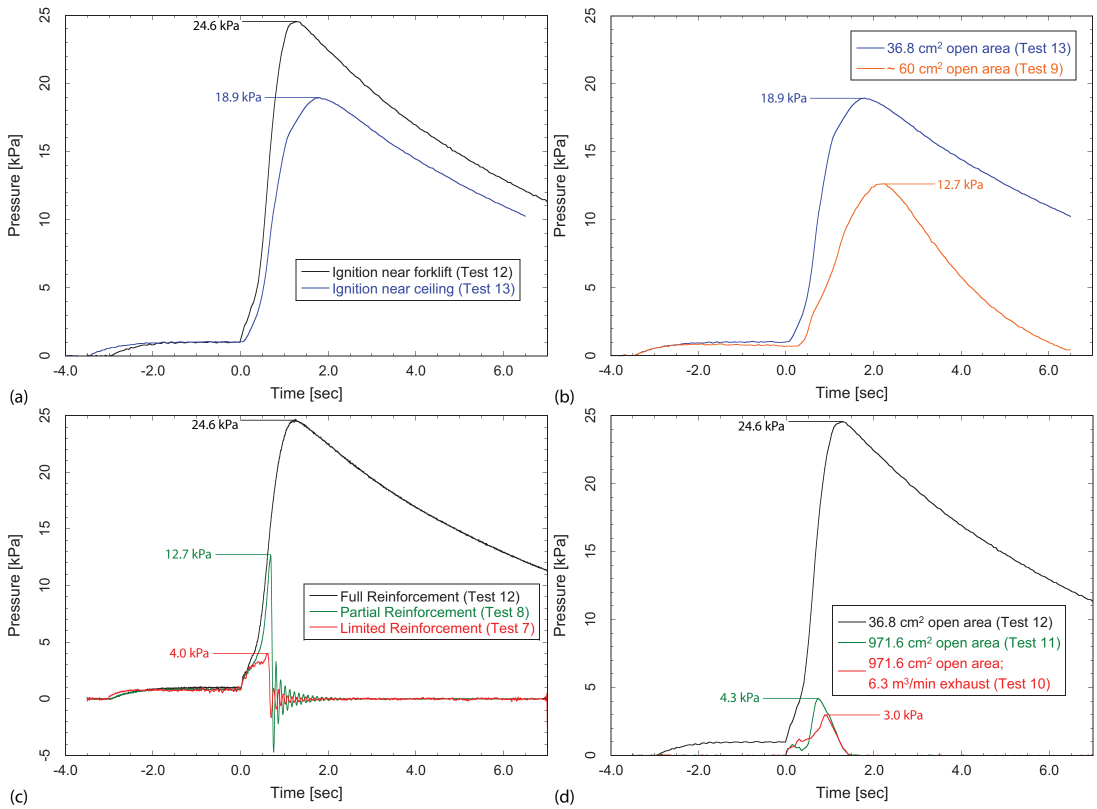

Figure 9. Warehouse overpressures comparison for (a) well-sealed conditions, (b) a moderate increase in leakage area, (c) inclusion of pressure relief panels, and (d) active/passive ventilation.

Table 4. Flame speed from flame front TOA measurements by the fast response thermocouples.

Test	-X [m/s]	+X	+Y
7	4.2	1.4	2.6
8	4.1	0.7	6.7
9	1.3	1.4	1.5
10	3.1	1.4	8.1
11	5.5	1.0	3.1
12	3.4	1.4	2.6
13	1.4	1.4	3.3

The peak measured overpressure during the test series was 24.6 kPa, which occurred for the well-sealed warehouse with a reinforced pressure relief panel and ignition near the forklift model (Test 12). Figure 9a shows that although the initial pressure rise resulted from the combustion of the H_2-rich plume above the forklift (observed from the IR video), a more substantial pressure increase followed once the ceiling mixtures ignited. Flame speeds in the -X (toward the back wall) and +Y directions (toward the right wall) were nearly double the flame speed in the +X direction. For the same warehouse configuration, but with ignition near the ceiling (Test 13), the peak overpressure was somewhat lower at 18.9 kPa, possibly due to leaner mixtures at the spark location. Relative to Test 12, measured flame speeds in the +X direction were roughly equivalent, but substantially decreased in the –X direction. The slower flame speeds conform to the slower flame front propagation observed with the IR imaging. Test 9 was identical to Test 13 except that a 5.08 cm internal diameter pipe on the facility was inadvertently left open to the outside. Since the pipe was closed during air leakage tests, the measured leakage area in Table 2 does not reflect the additional open area, and an effective leakage area of ~60 cm^2 is more representative. Figure 9b illustrates that the modest increase in open area led to noticeably slower pressure rise rates and 33% lower peak overpressures.

The inclusion of mitigation measures such as pressure relief panels, large ventilation areas, or mechanical exhaust were separately examined for scenarios with ignition near the forklift. Respective overpressures where the relief panels breached (Tests 7 and 8) were roughly one-sixth and one-half the peak overpressure reached for the well-sealed condition. Figure 9c indicates that once the relief panels were breached, internal overpressures rapidly exhausted and Helmholtz pressure oscillations with a 9.6-Hz frequency were observed. When the warehouse ventilation area was substantially increased (Test 11), the peak overpressure was reduced by 83% relative to the well-sealed condition. Furthermore, with the addition of mechanical exhaust (Test 10), the peak overpressure reduction was 87%. It should be cautioned, however, that the variation within peak pressures for the conditions with passive and active ventilation may be within the experimental variability. Pressure plots for both conditions (Fig. 9d) exhibit bimodal pressure peaks that are attributed to the two-stage ignition processes observed with the IR imaging and described for the well-sealed condition.

4 SUMMARY AND CONCLUSIONS

Dispersion and combustion data, based on an industry created FMEA for medium sized H_2 leaks from fuel cell powered forklift storage systems were gathered to support the development of validated modeling approaches that could be used to assess existing code guidelines. The release of 0.8 kg of H_2 into a 1,000 m^3 enclosure was simulated in a hardened subscale test facility located at the SRI Corral Hollow Experiment Site using Froude scaling relations to match the full scale release characteristics. Dispersion measurements from strategically placed concentration sensors indicated the transient release plume initially formed a momentum driven jet that was relatively insensitive to buoyancy, but quickly bent upwards as the storage tank pressure decreased. Lean H_2 ceiling mixtures were detected about 3 s into the release and by roughly 4 s no H_2 was detected near the release point. H_2/air mixtures rapidly spread along the ceiling and by 20 s were homogeneously distributed with mole fractions near the 4% lower flammability limit; it was unlikely these mixtures could be ignited beyond this time. Minimal dispersion variations were observed for conditions with and without mechanical exhaust.

Two spark points, located either 3 cm directly above the forklift vent or 10 cm below the ceiling, were selected based on an assessment of potential ignition sources. From the dispersion measurements, ignition delays of 3.0 and 3.5 seconds were selected for the forklift and ceiling ignition points respectively. Ignition kernel formation and flame propagation were imaged through the facility open end, while overpressure and flame speed measurements were recorded once the facility open end was replaced by a steel wall. For releases ignited near the forklift, the plume quickly burned and led to a moderate overpressure. This was followed 0.4 s later by a secondary ignition of accumulated ceiling H_2, which led to increased pressure rise rates and a 24.6 kPa peak overpressure. For the ceiling ignition scenario, lean mixtures at the spark location and the fact that plume mixtures were not ignited meant flame propagation was slower and pressure rise rates were less substantial. Slower pressure rise rates allowed more time for expanding gases to vent through the ~37 cm^2 leak area and for heat to transfer to the walls, which led to a 23% peak overpressure decrease. When the leakage area was further increased ~63%, the peak overpressure was reduced by 33%. If pressure relief panels were installed on the facility open end, overpressures rapidly exhausted once the panels were breached, and periodic Helmholtz oscillations were observed in the pressure data. For large effective leakage areas (972 cm^2), peak overpressures were reduced by 83% when ignition was near the forklift. Further decreases were observed when mechanical exhaust was included, but the impact was minor.

Using modeling approaches validated against the collected datasets, code development technical committees will have an improved technical basis to evaluate the effect of different code requirements on operational safety. Future work will analyze the impact of space reduction and turbulence enhancement that result from different shelving configurations on overall overpressure generation so that consequence modeling approaches can be further refined. Moreover, risk-informed technical assessments require quantitative information regarding accident frequency. Thus, probabilistic leak size and flow rate models are being developed to provide more comprehensive risk analysis tools.

5 ACKNOWLEDGMENTS

This research was supported by the United States Department of Energy, Office of Energy Efficiency and Renewable Energy, Fuel Cell Technologies Program, under the Safety, Codes, and Standards subprogram element managed by Antonio Ruiz. Sandia is operated by the Sandia Corporation, a Lockheed Martin Company, for the U.S. DOE under contract No. DE-AC04-94-AL8500.

REFERENCES

[1] LaChance J, Tchouvelev A, Engebo A, Development of uniform harm criteria for use in quantitative risk analysis of the hydrogen infrastructure. Int J Hydrogen Energy, 2011;36:59-66.
[2] NFPA 2, Hydrogen Technologies Code, National Fire Protection Agency, Quincy, MA, 2011.
[3] Houf WG, Evans GH, Ekoto IW, Merilo E, Groethe M, Hydrogen Fuel-Cell Forklift Vehicle Releases in Enclosed Spaces. Proc Int Conf Hydrogen Safety, San Francisco, CA, Sep 12-14, 2011.
[4] Swain MR, Filoso P, Grilliot ES, Swain MN, Hydrogen leakage into simple geometric enclosures. Int J Hydrogen Energy, 2003;28:229-48.
[5] Houf WG, Evans GH, James SC, Merilo E, Groethe M, Simulation of Hydrogen Releases from Fuel-Cell Vehicles in Tunnels. Proc World Hydrogen Energy Conf, Essen, Germany, May 16-21, 2010.
[6] Merilo EG, Groethe MA, Colton JD, Chiba S, Experimental study of hydrogen release accidents in a vehicle garage. Int J Hydrogen Energy, 2011;36:2436-44.
[7] Venetsanos AG et al., On the use of hydrogen in confined spaces: Results from internal project InsHyde. Int J Hydrogen Energy, 2011;36:2693-9.
[8] Swain MR, Swain MN, Passive ventilation systems for the safe use of hydrogen. Int J Hydrogen Energy, 1996;21:823-35.
[9] Molkov V, Dobashi R, Suzuki M, Hirano T, Venting of deflagrations: hydrocarbon-air and hydrogen-air systems. J Loss Prevent Proc, 2000;13:397-409.
[10] Baraldi D et al., An inter-comparison exercise on CFD model capabilities to simulate hydrogen deflagrations with pressure relief vents. Int J Hydrogen Energy, 2010;35:12381-90.
[11] Papanikolaou EA et al., HySafe SBEP-V20: Numerical studies of release experiments inside a naturally ventilated residential garage. Int J Hydrogen Energy, 2010;35:4747-57.
[12] Bauwens CR, Chaffee J, Dorofeev S, Effect of Ignition Location, Vent Size, and Obstacles on Vented Explosion Overpressures in Propane-Air Mixtures. Combust Sci Technol, 2010;182:1915-32.
[13] Zhang J, Delichatsios MA, Venetsanos AG, Numerical studies of dispersion and flammable volume of hydrogen in enclosures. Int J Hydrogen Energy, 2010;35:6431-7.
[14] NFPA 52, Vehicular Gaseous Fuel Systems Code, National Fire Protection Association, Quincy, MA, 2010.
[15] International Fire Code, International Code Council, Country Club Hills, IL, 2009.
[16] Astbury GR, Hawksworth SJ, Spontaneous ignition of hydrogen leaks: A review of postulated mechanisms. Int J Hydrogen Energy, 2007;32:2178-85.
[17] Hall DJ, Walker S, Scaling rules for reduced-scale field releases of hydrogen fluoride. J Hazard Mater, 1997;54:89-111.
[18] Winters WS, A New Approach to Modeling Fluid/Gas Flows in Networks. SAND2001-8422, Sandia National Laboratories, July, 2001.
[19] Moen CD, Evans GH, Domino SP, Burns SP, A Multi-Mechanics Approach to Computational Heat Transfer. Proc ASME Int Mech Eng Cong and Exhibition, New Orleans IMECE2002-33098, Nov. 17-22, 2002.
[20] FLACS Version 9.1 User's Manual, GEXCON, Bergen, Norway, 2010.